Available online at www.sciencedirect.com

ScienceDirect

Procedia Structural Integrity 41 (2022) 500–504

Structural Integrity Procedia

www.elsevier.com/locate/procedia

2nd Mediterranean Conference on Fracture and Structural Integrity

A novel methodology for fatigue assessment of Ductile Cast Iron (DCI) with solidification defects

Daniela Scorza[a]*, Camilla Ronchei[b], Sabrina Vantadori[c], Andrea Zanichelli[c], Andrea Carpinteri[c]

[a]*Department of Engineering, University of Naples Parthenope, Centro Direzionale Isola C4, 80143 Napoli, Italy*
[b]*Department of Civil Engineering, University of Calabria, via Pietro Bucci, 87036 Arcavacata di Rende (CS), Italy*
[c]*Department of Engineering & Architecture, University of Parma, Parco Area delle Scienze 181/A, 43124 Parma, Italy*

Abstract

In the present research work, the fatigue strength assessment of a DCI containing solidification defects is theoretically carried out by means of a procedure implementing: (i) a defect content analysis, (ii) the $\sqrt{area}$ -parameter model, and (iii) the multiaxial critical plane-based criterion by Carpinteri at al. An experimental campaign available in the literature, performed on DCI specimens under multiaxial fatigue loading, is analysed. The comparison between the obtained results and the experimental data shows a quite satisfactory agreement, highlighting the criterion accuracy.

© 2022 The Authors. Published by Elsevier B.V.
This is an open access article under the CC BY-NC-ND license (https://creativecommons.org/licenses/by-nc-nd/4.0)
Peer-review under responsibility of the MedFract2Guest Editors.

Keywords: Ductile Cast Iron (DCI); extreme value theory; fatigue assessment; fatigue strength; solidification defects

1. Introduction

Due to its advantageous mechanical properties (that is, high tensile strength, yield strength, elongation and toughness), when compared to gray iron and malleable iron, Ductile Cast Iron (DCI) is widely employed in several structural applications, such as critical automotive parts (as crankshafts), big engine blocks, parts of hydraulic presses, canisters for nuclear waste storage and wind turbines (Jenkins and Forrest, 1990). Such a DCI is a cast iron with a microstructure characterised by small spherical graphite particles embedded in a matrix, which is usually ferritic and/or

* Corresponding author. Tel.: +39 0521 905923; fax: +39 0521 905924.
E-mail address: daniela.scorza@uniparthenope.it

2452-3216 © 2022 The Authors. Published by Elsevier B.V.
This is an open access article under the CC BY-NC-ND license (https://creativecommons.org/licenses/by-nc-nd/4.0)
Peer-review under responsibility of the MedFract2Guest Editors.
10.1016/j.prostr.2022.05.056

pearlitic, depending on alloy composition, casting control and final heat treatment. When DCIs are employed in heavy section components casting, thus involving long solidification times, the microstructure quality of DCIs cannot be properly controlled with the consequent introduction of material intrinsic defects, named also solidification defects (Borsato et al., 2018.). Such defects, which may be non-nodular graphite elements, non-metallic inclusions, slag inclusions, and macro-/micro-shrinkage porosities, have a detrimental effect on the DCI fatigue properties, which has to be taken into account in fatigue strength assessment of heavy section DCI components. Therefore, a procedure for such an assessment is here proposed by implementing: (i) a defect content analysis, (ii) the $\sqrt{area}$ -parameter model, and (iii) the multiaxial critical plane-based criterion by Carpinteri at al. (Carpinteri et al., 2015; Vantadori et al., 2020).

Nomenclature

$\bar{I}$, T	error index mean value and return period, respectively
V , V_0	useful cross-section volume and standard inspection volume, respectively
$\sigma_{af,-1}$, $\tau_{af,-1}$	experimental fatigue strengths under fully reversed normal and shear stresses, respectively
$\sigma_{eq,a}$	equivalent uniaxial stress amplitude
σ_w , τ_w	computed fatigue strengths under normal and shear stresses, respectively

2. Examined experimental campaign

The experimental campaign (Endo, 2000), hereafter examined, was performed on a ferritic DCI with 14% graphite nodules in a white ferrite matrix, named DCI EN-GJS-400-18 according to the European designation (FCD400 in the original Japanese designation). Its ultimate tensile strength is equal to 418 MPa, elongation at failure equal to 25.0 % and Vickers hardness equal to 186. Small cylindrical specimens were subjected to both uniaxial (tension or torsion) and biaxial (combined tension and torsion) cyclic loading with a constant amplitude (Endo and Yanase, 2014). The fatigue tests were characterised by loading ratio R equal to -1, and three values of the ratio between shear and normal stress amplitudes were considered, that is, $\tau_{xy,a}/\sigma_{x,a} = 0$, 1 and ∞. The phase shift, β, between axial and torsional loading, was either 0° or 90°. The fatigue data related to the above experimental campaign are listed in Table 1. The run-out condition was assumed when a specimen survived more than 10^7 cycles, whereas the failure condition was defined when the crack was visually observed during the test. From the uniaxial fatigue data, the fully reversed normal and shear fatigue limits were computed as $\sigma_{af,-1} = 205\ MPa$ and $\tau_{af,-1} = 175\ MPa$, respectively.

Table 1. Fatigue data of the experimental campaign reported in Endo (2000) and Endo and Yanase (2014).

Test No.	β (°)	$\sigma_{x,a}$ (MPa)	$\tau_{xy,a}$ (MPa)	
1	-	195	-	*Run-out*
2	-	200	-	*Run-out*
3-4	-	205	-	*Run-out*
5	-	210	-	*Failure*
6	-	220	-	*Failure*
7	-	-	165	*Run-out*
8	-	-	175	*Run-out*
9	-	-	180	*Failure*
10	-	-	185	*Failure*

Test No.	β (°)	$\sigma_{x,a}$ (MPa)	$\tau_{xy,a}$ (MPa)	
11	0	115	115	*Run-out*
12	0	120	120	*Run-out*
13	0	125	125	*Failure*
14	0	130	130	*Failure*
15	90	120	120	*Run-out*
16	90	130	130	*Run-out*
17	90	135	135	*Failure*
18	90	140	140	*Failure*
19	90	160	160	*Failure*

3. Proposed procedure for fatigue strength assessment

Now, the proposed procedure is outlined and applied to the above experimental campaign by implementing: (i) a defect content analysis, (ii) the $\sqrt{area}$ -parameter model and (iii) the multiaxial critical plane-based criterion by Carpinteri at al.

3.1. Defect content analysis

The defect content analysis is performed according to the extreme value theory (Murakami et al., 1988; Murakami et al., 1994). The distribution of the defects (macro-/micro-porosities in this case) was determined by examining a fracture surface, normal to the specimen longitudinal axis, by using a Scanning Electron Microscope with an inspection area equal to 0.5 mm^2. The largest defect was determined inside such an area and the inspection was repeated 50 times on the examined surface (Endo and Yanase, 2014). The measured square root area values $\sqrt{area}_j$ are listed in ascending order and the probability graph is plotted in Figure 1(a), showing a linear trend.

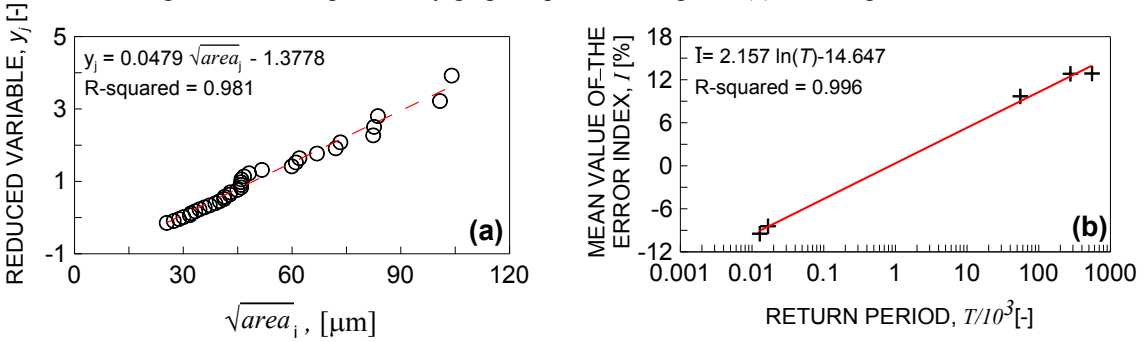

Fig. 1. (a) Probability graphs of the defect distribution according to the extreme value theory; (b) error index mean value vs return period, T .

Once the return period $T = V/V_0$ is properly set, the value of the square root of the expected maximum defect size, $\sqrt{area}_{max}$, may be written as function of T as follows:

$$\sqrt{area}_{max} = \frac{1}{0.0479} y + \frac{1.3778}{0.0479} \quad \text{with} \quad y = -ln\left[-ln\left(\frac{T-1}{T}\right)\right] \tag{1}$$

where V is the useful cross-section volume and V_0 is the standard inspection volume.

3.2. $\sqrt{area}$ -parameter model

The fatigue limits under normal loading, σ_w, and shear loading, τ_w, are computed according to Murakami and Yanase formulations (Murakami, 2002; Yanase and Endo, 2014), respectively, by assuming the presence of the defect just below the surface:

$$\sigma_w = \frac{1.41(HV + 120)}{\left(\sqrt{area}_{max}\right)^{\frac{1}{6}}} \tag{2a}$$

$$\tau_w = \frac{1.19(HV + 120)}{\left(\sqrt{area}_{max}\right)^{\frac{1}{6}}} \tag{2b}$$

3.3. Multiaxial critical plane-based criterion by Carpinteri at al.

The fatigue strength assessment is finally performed, according to the multiaxial critical plane-based criterion by Carpinteri et al. (Carpinteri et al., 2015; Vantadori et al., 2020). First, the orientation of the critical plane is determined by means of an off-angle, $\delta = 3/2 \cdot \left[1 - \left(\tau_w/\sigma_w\right)^2\right] \cdot 45°$, formed by the normal to the critical plane and the averaged direction of the maximum principal stress. Therefore, the multiaxial fatigue limit condition is expressed by the following non-linear combination of the equivalent normal stress amplitude $N_{eq,a}$ and the shear stress amplitude C_a acting on the above critical plane:

$$\left(N_{eq,a}/\sigma_w\right)^2 + \left(C_a/\tau_w\right)^2 = 1 \quad \text{with} \quad N_{eq,a} = N_a + \sigma_w\left(N_m/\sigma_u\right) \tag{3}$$

where N_m and N_a are the mean value and the amplitude of the normal stress, respectively, and σ_u is the material ultimate tensile strength. From Eq. (3), an equivalent uniaxial normal stress amplitude $\sigma_{eq,a}$ is defined as follows:

$$\sigma_{eq,a} = \sqrt{N_{eq,a}^2 + \left(\sigma_w/\tau_w\right)^2 C_a^2} \tag{4}$$

The accuracy of the fatigue strength assessment is evaluated through the following error index:

$$I = \frac{\sigma_{eq,a} - \sigma_w}{\sigma_w} \cdot 100 \tag{5}$$

3.4. Optimisation procedure

The above procedure provides for the optimisation of the return period, T, allowing to obtain an error index mean value equal to zero (Vantadori et al., 2021; Vantadori et al., 2022). Since such a return period is defined as the ratio between the useful cross-section volume V and the standard inspection volume V_0 (here equal to $2.55 \cdot 10^{-2}\ mm^3$), five values of V are considered. For each value of the return period, the fatigue strength assessment is performed by using the computed fatigue strengths and the corresponding error index mean value is determined (Table 2). Then, such error indexes are plotted against T in Figure 1(b), and the points are interpolated by a logarithmic curve, whose expression is here reported:

$$\bar{I} = 2.157 ln(T) - 14.647 \tag{6}$$

The optimal return period T_{opt} (and the related $V_{opt} = 22.7\ mm^3$) is determined for $\bar{I} = 0$, and the fatigue strengths are computed as $\sigma_w = 183.22\ MPa$ and $\tau_w = 154.64\ MPa$. Finally, the last fatigue assessment is performed.

Table 2. Useful cross-section volume, return period, square root of the maximum defect size, fatigue strengths and error index mean value.

Prediction volume		T	$\sqrt{area}_{\max}$	σ_w	τ_w	$\bar{I}$
Symbol	Size (mm^3)	(-)	(μm)	(MPa)	(MPa)	(%)
$V_{\tau_{af,-1}}$	$3.21 \cdot 10^{-1}$	$1.28 \cdot 10^{1}$	81.17	207.35	175.00	–9.47
$V_{\sigma_{af,-1}}$	$4.27 \cdot 10^{-1}$	$1.67 \cdot 10^{1}$	86.92	205.00	173.01	–8.44
V_1	$1.41 \cdot 10^{3}$	$5.54 \cdot 10^{4}$	256.77	171.14	144.44	9.68
V_5	$7.07 \cdot 10^{3}$	$2.27 \cdot 10^{5}$	290.37	167.67	141.51	12.82
V_{10}	$1.41 \cdot 10^{4}$	$5.54 \cdot 10^{5}$	304.84	166.31	140.36	12.86
V_{opt}	$2.27 \cdot 10^{1}$	$8.89 \cdot 10^{2}$	170.51	183.22	154.64	–

4. Results and discussion

The results in terms of stress components are plotted in Figures 2 for all data being examined by applying both the proposed procedure (Fig. 2(a)) and the Carpinteri et al. criterion, that is, by employing the experimental fatigue limits (Fig. 2(b)). The fatigue endurance condition, given by Eq. (3), defines an ellipse in the $N_{eq,a}$ - C_a plane.

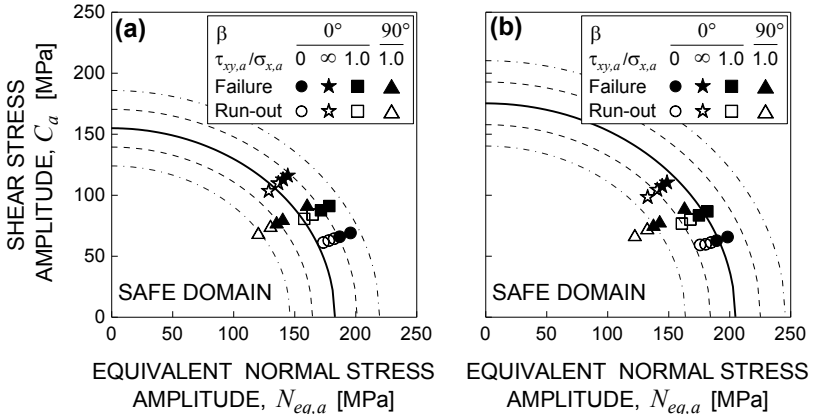

Fig. 2. Shear stress amplitude vs equivalent normal stress amplitude determined by employing the: (a) present procedure and (b) the Carpinteri et al. criterion with the experimental fatigue strength values

The dashed lines correspond to an error band equal to $\pm 10\%$, whereas the dash-dot lines to an error band equal to $\pm 20\%$. We can observe that, according to the present procedure, the estimations are conservative and in agreement with the experimental evidence for the in-phase loading, whereas they are not conservative for out-of-phase loading although the points representing failures fall within the -20% scatter band. On the contrary, the Carpinteri at al. criterion provides more non-conservative results.

Finally, only the tests which experiment failure are considered and the equivalent stress amplitude is plotted in Figure 3. The results obtained through the present procedure are represented by both the symbols and the line in red, whereas the $\sigma_{eq,a}$ values computed according to the Carpinteri et al. criterion and the line representing the experimental fatigue strength are plotted in blue. It can be noted that, when the present procedure is applied, 78% of the estimations are conservative, whereas only 22% of them are conservative according to the Carpinteri et al. criterion.

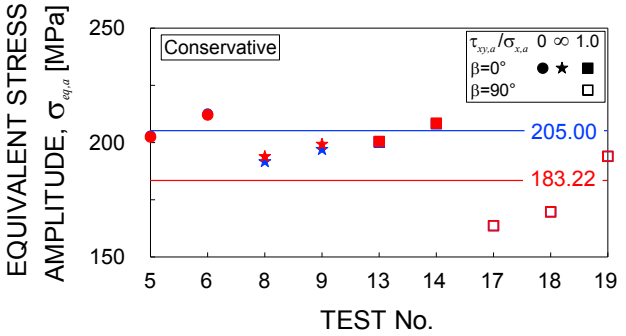

Fig. 3. $\sigma_{eq,a}$ against the test No., according to the present procedure (in red) and the Carpinteri et al. criterion (in blue).

5. Conclusions

A procedure for fatigue strength assessment of a ductile cast iron with solidification defects is here proposed and applied to the data of an experimental campaign available in the literature. A content analysis has been performed according to the extreme value theory and the value of the $\sqrt{area}_{max}$ has been obtained after an optimisation of the return period. The results, in terms of endurance strength assessment, are quite satisfactory, highlighting the good accuracy of the present procedure.

References

Borsato, T., Ferro, P., Berto, F., 2018. Novel method for the fatigue strength assessment of heavy sections made by ductile cast iron in presence of solidification defects. Fatigue and Fracture of Engineering Materials and Structures 41, 1746-1757.

Carpinteri, A., Ronchei, C., Scorza, D., Vantadori, S., 2015. Critical Plane Orientation Influence on Multiaxial High-Cycle Fatigue Assessment. Physical Mesomechanics 18, 348-354.

Endo, M., 2000. Fatigue strength prediction of ductile irons subjected to combined loading, Proc. of ECF13.

Endo, M., Yanase, K., 2014. Effects of small defects, matrix structures and loading conditions on the fatigue strength of ductile cast irons. Theoretical and Applied Fracture Mechanics 69, 34-43.

Jenkins, L.R., Forrest, R.D., 1990. Properties and Selection: Irons, Steels, and High-Performance Alloys, Vol 1, ASM Handbook. 10th ed. ASM International, Metals Handbook.

Murakami, Y., 2002. Metal Fatigue: Effects of Small Defects and Nonmetallic Inclusions. Oxford, UK: Elsevier Science Ltd.

Murakami, Y., Kodama, S., Konuma S., 1988. Quantitative Evaluation of Effects of Nonmetallic Inclusions on Fatigue Strength of High Strength Steel. Transactions of the Japan Society of Mechanical Engineers Series A 500, 688-696.

Murakami, Y., Toriyama, T., Coudert, E.M., 1994. Instructions for a new method of inclusion rating and correlations with the fatigue limit. Journal of Testing and Evaluation 22, 318–326.

Vantadori, S., Carpinteri, A., Luciano, R., Ronchei, C., Scorza, D., Zanichelli, A., Okamoto, Y., Saito, S., Itoh, T., 2020. Crack initiation and life estimation for 316 and 430 stainless steel specimens by means of a critical plane approach. International Journal of Fatigue 138, 105677.

Vantadori, S., Ronchei, C., Scorza, D., Zanichelli, A., Carpinteri, A., 2021. Fatigue behaviour assessment of ductile cast iron smooth specimens. International Journal of Fatigue 152, 106459.

Vantadori, S., Ronchei, C., Scorza, D., Zanichelli, A, Araújo, L.C., Araújo, J.A., 2022. Influence of non-metallic inclusions on the high cycle fatigue strength of steels. International Journal of Fatigue 154, 106553.

Yanase, K., Endo, M., 2014. Multiaxial high cycle fatigue threshold with small defects and cracks. Engineering Fracture Mechanics 123, 182–196.